Planetary and Space Science 57 (2009) 350–363

Contents lists available at ScienceDirect

Planetary and Space Science

journal homepage: www.elsevier.com/locate/pss

Martian gravity field model and its time variations from MGS and Odyssey data

J.C. Marty [a,*], G. Balmino [a], J. Duron [b,1], P. Rosenblatt [b,1], S. Le Maistre [b,1], A. Rivoldini [b,1], V. Dehant [b,1], T. Van Hoolst [b,1]

[a] Centre National d'Etudes Spatiales, 18, Avenue Edouard Belin, 31401 Toulouse Cedex 9, France
[b] Observatoire Royal de Belgique, 3, Avenue Circulaire, 1180 Brussels, Belgium

ARTICLE INFO

Article history:
Received 8 September 2008
Received in revised form
17 December 2008
Accepted 9 January 2009
Available online 29 January 2009

Keywords:
Mars
Dynamical geodesy
Global gravity field
Time variations

ABSTRACT

We present results of several years of research and data processing aimed at modelling the Mars gravity field and its longest wavelength time variations. The new solution includes tracking data from Mars Global Surveyor (MGS) from 1998 to 2006 (end of mission) and from Mars Odyssey from 2002 to the spring of 2008; this is the longest analyzed data set from these two orbiter missions as compared to previous works. The new model has been obtained by a team working in Europe, independently from the works of groups at NASA Jet Propulsion Laboratory (JPL) and Goddard Space Flight Center (GSFC), also with totally independent software. Observations consist in two and three-way Doppler measurements (also one way for MGS), and range tracking data collected by the Deep Space Network and have been processed in 4 day arcs, taking into account all disturbing forces of gravitational and non-gravitational origins; for each arc the state vector, drag and solar pressure model multiplying factors, and angular momentum dump parameters are adjusted. The static field (MGGM08A) is represented in spherical harmonics up to degree and order 95 and is very close to previously published models (in terms of spectral components and also over specific features); correlations with the global Mars topography are established and apparent depths of compensation by degree are derived. Lumped zonal harmonics of degree two and three are solved for every 10 days, exhibiting variations in line with previous results (including authors' ones); the work also shows the difficulty of finding clean signatures (annual and semi-annual) for the zonal coefficient of second degree. The k_2 Love number is also derived from the ensemble of data, as well as from subsets of them; values between 0.110 and 0.130 are found, which are consistent with the existence of a Martian fluid core of significant radius.

1. Introduction

In the context of the highly renewed interest to Mars the need for increasing our knowledge of various geodetic and geophysical quantities related to the history and present state of the red planet is obvious. Among these are parameters describing its gravitational potential since this reflects the global and regional density distribution. Until a network of seismometers is developed on the surface of Mars, gravity, topography and rotation are best at providing clues about its interior.

The gravity field is modelled by a spherical harmonic series, written at each point P as

$$U = \frac{GM}{r} \sum_{l=2}^{l=L} \left(\frac{R}{r}\right)^{l} \sum_{m=0}^{+l} (C_{lm} \cos m\lambda + S_{lm} \sin m\lambda) P_{lm}(\sin \varphi) \quad (1)$$

where G is the gravitational constant, M the mass of Mars, R the equatorial reference radius, C_{lm} and S_{lm} are the dimensionless harmonic coefficients of degree l and order m, and r, φ, λ are the spherical coordinates of the point P in a reference system fixed with respect to the planet; the P_{lm}'s are the Legendre functions of the first kind (polynomials when $m = 0$); these functions and all harmonic coefficients are here normalized as in Kaula (1966). In the present work we used GM and R with the following values: $4.2828375 \times 10^{13}\,\mathrm{m^3\,s^{-2}}$ and $3.396 \times 10^{6}\,\mathrm{m}$, respectively. The summation, which starts at degree 2 if one assumes that the reference system origin coincides with Mars center of mass, is in principle infinite but it is in practice truncated to a maximum degree and order L predetermined by sensitivity analysis based on the orbit characteristics and tracking system capabilities.

* Corresponding author. Tel.: +33 5 61 33 2980.
E-mail addresses: jean-charles.marty@cnes.fr (J.C. Marty), balmino@dtp.obs-mip.fr (G. Balmino), Julien.Duron@hotmail.com (J. Duron), P.Rosenblatt@oma.be (P. Rosenblatt), Sebastien.LeMaistre@oma.be (S. Le Maistre), Attilio.Rivoldini@oma.be (A. Rivoldini), V.Dehant@oma.be (V. Dehant), Tim.Vanhoolst@oma.be (T. Van Hoolst).
[1] Tel.: +32 2 373 67 32.

0032-0633/$ - see front matter © 2009 Elsevier Ltd. All rights reserved.
doi:10.1016/j.pss.2009.01.004

The C_{l0} coefficients are called zonals, the C_{lm}, S_{lm} $(m>0)$ are the tesseral harmonics with the sectorials ($l=m$) being a special subclass. In principle they may all vary with time due to mass exchange between the atmosphere and the polar caps principally at seasonal time scales.

Although many global models of the Martian gravity field exist, including time variations of the longest wavelength features (represented by low degree and order harmonics), the accumulation of new data from the tracking of the current Mars orbiters makes it necessary to use such data in most up to date solutions. The old Mariner 9 and Viking 1 and 2 S-band data sets proved very valuable at a time; many years after works which were limited by computer power and tracking system performances (Balmino et al., 1982) new spherical harmonic models to $L=50$ could be derived — although with large uncertainties in the high degree terms: GMM1 (Smith et al., 1993), Mars50c (Konopliv and Sjogren, 1995). But the much higher quality of the modern X-band data from the Mars Global Surveyor (MGS) and Mars Odyssey (ODY) missions makes the old data quasi obsolete. The early phases of the MGS mission already enabled the determination of much more detailed gravity models early in the mission (Sjogren et al., 1999; Smith et al., 1999a; Tyler et al., 2001). The excitement grew when, for the first time, the predicted time variations of the long wavelength gravity field of Mars (Smith et al., 1999b) could indeed be determined; several solutions of these variations, limited to those of the second and third degree zonal harmonics, were produced by different methods (Smith et al., 2001a; Smith and Zuber, 2003; Yoder et al., 2003).

Refinements came from the collection and processing of more data; for instance the NASA Goddard Space Flight Center (GSFC) team derived the GMM-2B model to degree and order $L=80$ (Lemoine et al., 2001), then GGM1041C complete to $L=90$ (see Planetary Data System Geosciences Node, http://www.pds.wustl.edu); in addition to the classical Doppler and range tracking measurements, the GSFC models include altimeter crossover data formed from the Mars Orbiter Laser Altimeter (MOLA, see Neumann et al., 2001). At the same time a team at NASA Jet Propulsion Laboratory (JPL) derived several solutions of increasing resolution (i.e. increasing L). The latest published model, MGS95J (Konopliv et al., 2006), used 6 years of MGS tracking data plus 3 years of measurements on the Mars Odyssey (ODY) spacecraft which meanwhile had been put in orbit; this is a solution up to $L=95$, which also includes seasonal changes in the second and third degree zonal harmonics as well as in the tesseral coefficients of degree two and three and of order one. In addition the Love number of degree two, the mass of the Martian moons and the masses of five asteroids (to which the analyzed orbits were sensitive) have been determined.

Our work has consisted in doing similar modelling of the gravity field of Mars, the goal being not only to reproduce any of the previous solutions with an independent software but: (i) to try to enhance the quality of the model by processing a longer data set; (ii) to show the sensitivity of some retrieved parameters (especially the time-varying ones and Love number) to some processing features and strategies (see next section). This paper is a synthesis of our efforts over several years in trying to improve our modelling of the static (mean) Martian gravity field and its major time variations (Balmino et al., 2005; Duron et al., 2006, 2007).

2. Spacecraft data and processing characteristics

The two mission orbits have very close characteristics in terms of mean metric elements (a: semi-major axis, e: eccentricity, I: inclination); these are (3768 km, 0.01, 92.9°) for MGS, and (3796 km, 0.01, 93.1°) for ODY, which give them similar capabilities at gravity mapping as seen in Fig. 1. However the angle between the orbital planes (~100° during the considered time span) gives them a different sensitivity at a given time (and as seen from the Earth) to some harmonic coefficients such as the first even and odd degree zonals (Yoder et al., 2003); this also induces some phase differences in the surface forces (besides differences in the spacecraft element geometries and characteristics) thus the advantage of using both orbiters simultaneously in the inverse problem.

We have analyzed most tracking data collected by the Deep Space Network (DSN) over the MGS orbital mission (until it ended in November 2006) and since the beginning of the ODY mission (until end of March 2008). Of these we retained for the present work: (i) the MGS-Gravity Calibration Orbit (GCO) plus all mapping phases data (since February 20, 1999), and (ii) the mapping phases data of ODY (not the transition phase).

These data consist in one-way Doppler from MGS, of two and three-way ramped Doppler and also two-way range measurements for MGS and ODY, all in X band and acquired by the DSN stations at the three sites of Goldstone, Madrid, and Canberra. The averaging time for the Doppler data was 10 s. Table 1 summarizes the amount of data retained in the gravity solution. These observations were processed in arcs of approximately 4 days duration each. We used the software, called GINS (Géodésie par Intégrations Numériques Simultanées), which is developed by the CNES in collaboration with ROB for planetary geodesy applications, and is totally independent from software used by the NASA JPL and GSFC teams.

The precise orbit determination (POD) and the retrieval of the physical parameters are based on a full dynamical approach using the numerical integration of the equations of motion (and associated variational equations) combined with a least squares adjustment of the unknowns which enter in the linearized observation equations.

The processing of the observations and the orbit dynamic modelling are done according to the following:

- DE414 planetary ephemeris (Standish, 2006, documented in Konopliv et al., 2006);
- Martian precession is as in Konopliv et al. (2006); nutations are from Folkner et al. (1997) and prime meridian of Mars consistent with the IAU 2000 conventions at epoch J2000 (Seidelmann et al., 2002); seasonal spin variations are not taken into account;
- Earth kinematics, polar motion, solid and ocean tide loading effects according to the IERS standards (McCarthy, 1996); Earth atmosphere loading effect at tracking stations uses the Gegout (personal communication, 1996) formulation with the 6-h pressure grids from the ECMWF (obtained via special agreement);
- the initial Martian gravitational model is JGM95J01, a static solution also referred to as MGS95J (Konopliv, *private communication*), complete to degree and order 95;
- third body attraction due to the Sun, Moon and planets uses the DE414 ephemeris and constants; for the attraction of the Martian satellites Phobos and Deimos we make use of the ephemeris developed by Lainey et al. (2007); the solid tide effect due to k_2 is computed with an initial value of 0.1; the tidal effect of Phobos on Mars is not considered.
- surface forces consist in: atmospheric drag which is evaluated with a semi-empirical Drag Temperature Model (DTM; Bruinsma and Lemoine, 2002); direct solar pressure, indirect reflected solar radiation from Mars and radiation pressure from the Mars thermal emission, the latter being modelled according to Lemoine (1992);

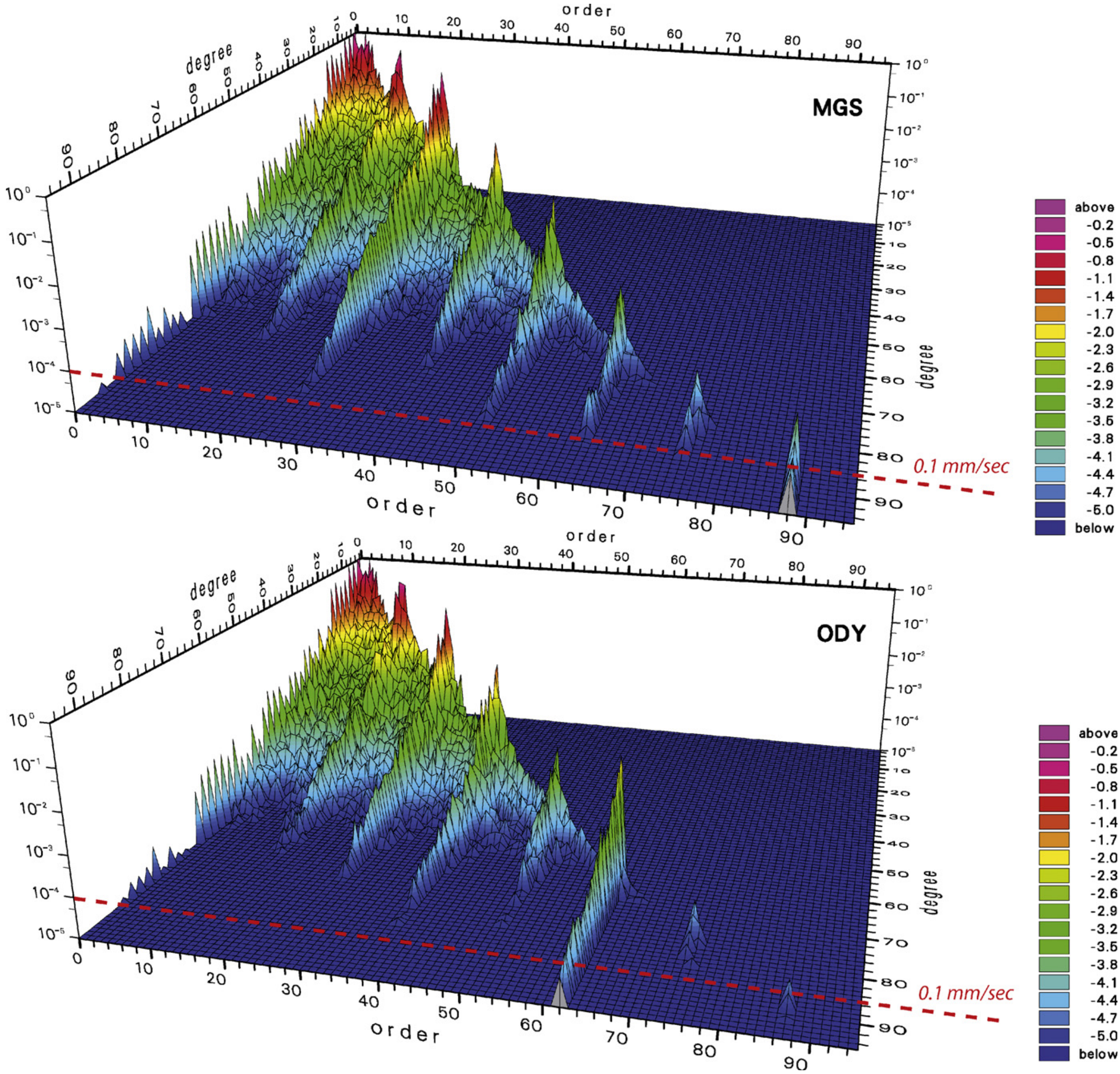

Fig. 1. Diagram of Mars gravity orbital effects on MGS and ODY (linear theory), shown as velocity perturbations for C_{lm}, S_{lm} pairs. The color scale is for the decimal logarithm of the perturbation in m/s. The 0.1 mm/s dotted line corresponds to about twice the ultimate capabilities of the tracking system in X band. Note the resonance bands which slightly differ as the orders increase, and the different perturbation amplitudes.

Table 1
Summary of processed data.

	MGS	ODY
One-way doppler	2,453,466	–
Two-way doppler*	3,404,147	4,105,820
Three-way doppler*	136,576	466,289
Two-way range	33,430	53,904
Number of arcs (arc length ~4 days)	428	348

The time periods covered are for MGS February 4, 1999–November 2, 2006, and for ODY January 11, 2002–January 14, 2002 (transition orbit 200 × 500 km) and March 27, 2002–March 30, 2008. The number of arcs are those which have been retained in the MGGM08A model.

- empirical accelerations are modelled over the duration of each angular momentum desaturation (AMD) event according to information provided by the project, and we solve for a delta acceleration vector for each such event;
- relativistic effects on the measurements (i.e. delays on ranges and differenced-range Doppler, and frequency modification) and on the spacecraft dynamics (e.g. the Schwarzschild effect) are based on the parameterized post-Newtonian formulation; time transformations, between coordinate and atomic time scales, are done as in Moyer (2000);
- surface forces modelling uses macro-models of the MGS (Lemoine, personal communication) and ODY (Konopliv,

personal communication) spacecraft decomposed into a bus (parallelepiped), solar panels (flat plates) and parabolic high gain antenna, with coefficients for the specular and diffuse properties of each surface element; the attitude of each spacecraft and of its articulated panels and antenna in inertial space is known from sets of quaternions provided by the project — or sometimes modelled analytically when information is missing; a peculiarity of the ODY spacecraft elements configuration is the occurrence of solar pressure self-shadowing at times (Mazarico et al.) which we have modelled in a general manner (for all surface forces).

- other corrections to the measurements include: the tropospheric delay which makes use of the meteorological data collected every half-hour at the DSN sites or coming from ECMWF 6-h grids of pressure, temperature and humidity since 2001, antenna phase center from the DSN stations, antenna offsets which are peculiar to each spacecraft and mission phase; these corrections include center of mass offsets provided with respect to the spacecraft body-fixed coordinate system.

We solve for the following parameters:

- the initial state vector components at epoch for each arc;
- empirical multiplying factors, F_D, for the drag acceleration (one per day — instead of the once per revolution strategy in our earlier work) accounting for the model imperfections;
- empirical multiplying factors, F_S, for the solar radiation pressure (one per arc) also accounting for the model imperfections;
- empirical delta accelerations at the AMD epochs (not precisely known). A priori uncertainties are the following: for MGS 5.10–5 m/s^2 and for ODY 1.10–5 m/s^2. A priori values have been taken into account for ODY only;

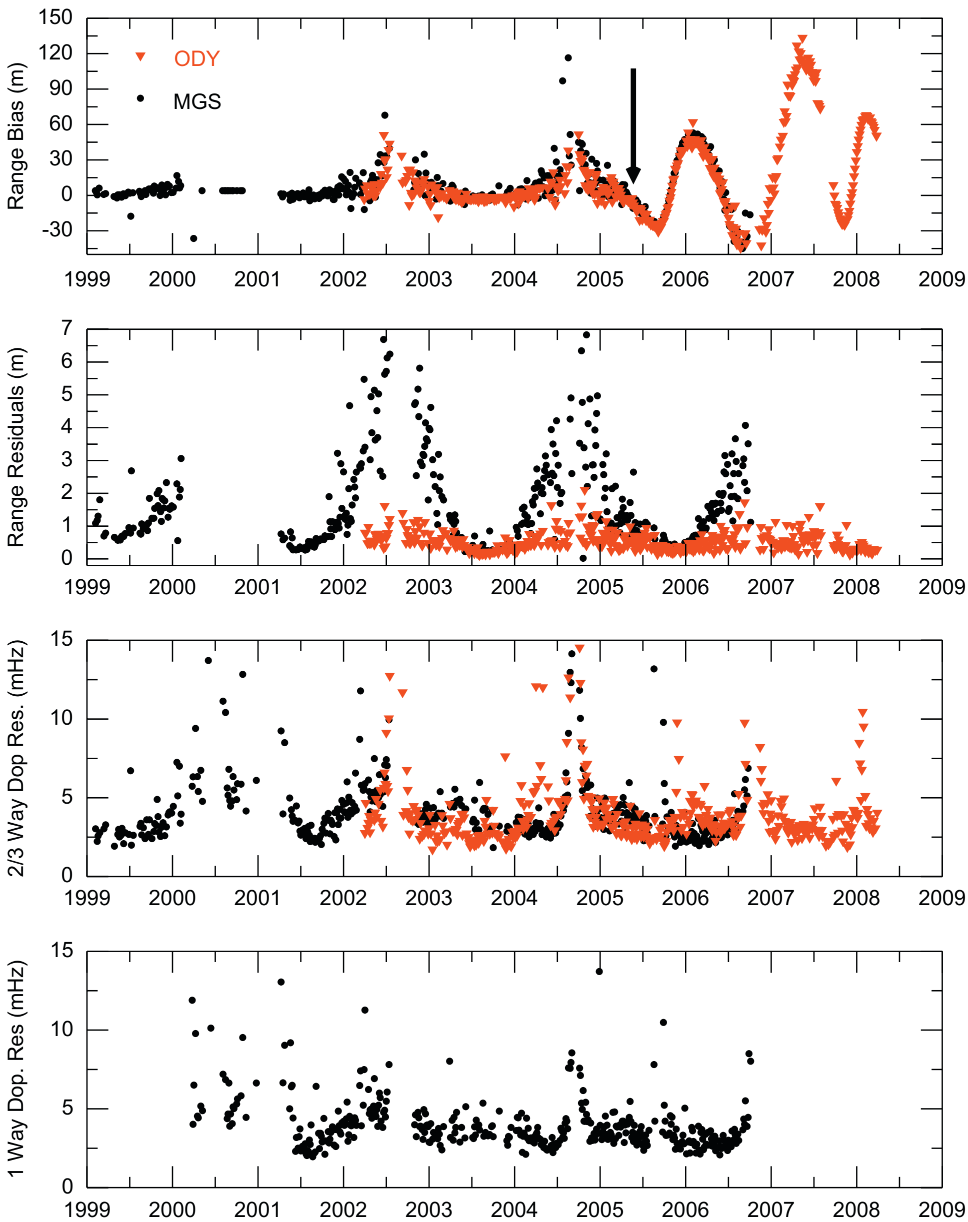

Fig. 2. History of the MGS and ODY orbit quality fits in terms of RMS residuals of range and Doppler measurements; the latter are given in millihertz (multiply by 0.035 and 0.0175 for one and two or three-way Doppler, respectively, to obtain residuals in mm/s). Range residuals are smaller for ODY than for MGS, which is unexplained Also shown are the range biases which behaviour after April 2005 (vertical arrow) corresponds to the latest data included in DE414 ephemeris.

- for each arc, one bias per DSN station for two or three-way Doppler measurements (found to be very small for two-way, as expected);
- one bias per arc for one-way Doppler measurements accounting for the USO stability uncertainty or the possible ephemeris errors (no drift estimate);
- one bias per DSN station and per arc for the ranging measurements accounting, in addition to the ephemeris errors, for the uncertainties on the DSN antenna center position or the instrumental delays (such as the range group delay of the transponder);
- gravity harmonics up to degree and order 5, at 10 day intervals (with the possibility to solve for a mean value over the whole period, or sub-periods);
- other gravity harmonics up to degree and order 95;
- Love number k_2.

Due to correlations which may be high between some of these parameters — and lack of observability in some instances, a priori variances are input (as additional equations in the least squares procedure) to stabilize the inversion; this is specially critical for the AMD empirical delta accelerations which impact the consistency of part of the solution.

We ran a large number of solutions, with MGS data alone, with ODY data alone, with the whole data set, with the MGS data subset corresponding to November 2002–November 2006, etc. These solutions were basically of three types:

- *type 1 solutions*: all the above parameters are determined in ensemble (the time-varying part being limited to the zonal harmonics of degrees 2 and 3),
- *type 2 solutions*: we solve for all parameters, but without time variations (and with or without k_2),
- *type 3 solutions*: we solve for all parameters but the static field.

The time-varying coefficients are always estimated at 10 days interval.

Variants were also considered, for instance in varying the a priori uncertainties on some parameters, or by linking the time-variable gravity coefficients in forcing them to be periodic (with a priori periods).

3. Orbit computation results

The quality of the orbit adjustment, seen over the whole processed period, gives some indication on the quality of the physical model itself despite the number of empirical parameters which are introduced.

The observation residuals for the two missions are shown in Fig. 2 for each measurement type. Characteristic patterns associated with solar conjunctions are, as usual, due to insufficient modelling of the solar plasma correction. Aside from these, the residuals are at the 2–5 mHz level in Doppler and around 0.5 m in range. For the latter it is worth noting the behaviour of the range bias which increases significantly (with a definite pattern) after April 2005; it corresponds to the date of the last MGS and ODY range data which have been included in the DE114 ephemeris. The same pattern has also been found from the range tracking data of the Mars Express spacecraft (Rosenblatt et al., 2008).

The surface forces coefficients history shown in Fig. 3 is obtained with the parameterization and models described in

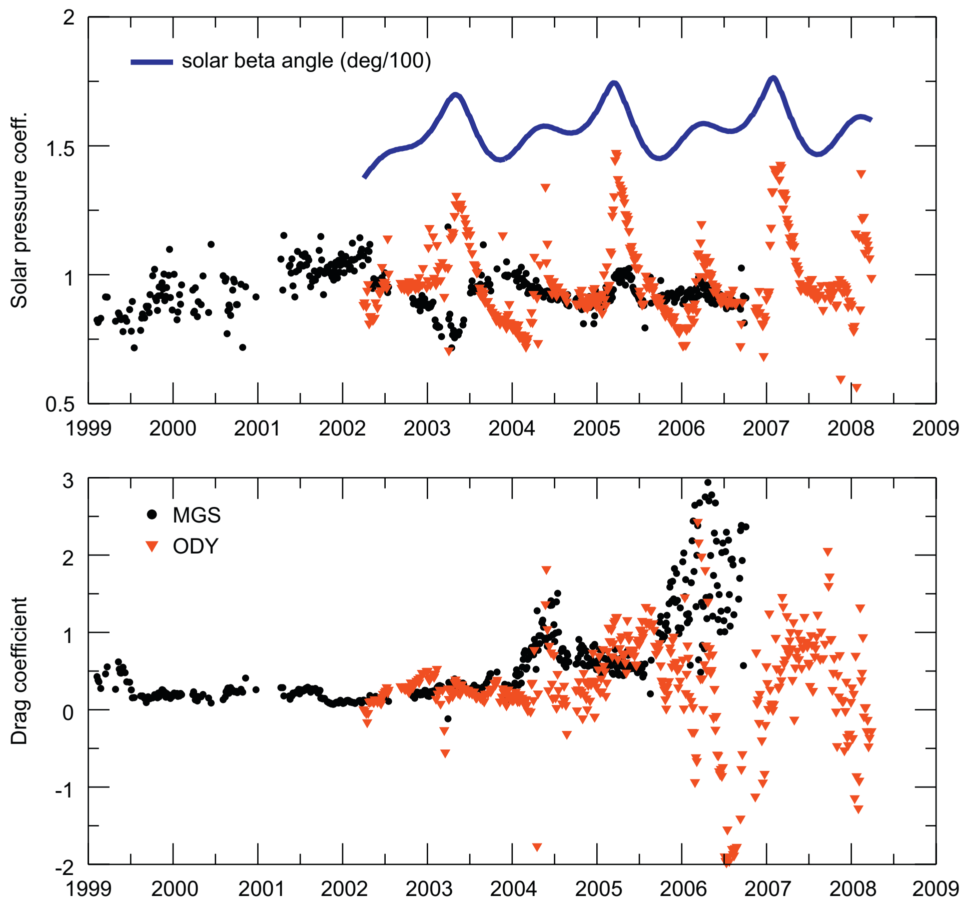

Fig. 3. Solar pressure and drag coefficient history.

Section 2. A priori values of 1 ± 1 were adopted for both coefficients.

The solar pressure coefficients have variations which follow those of the solar "beta" angle (the angle between the orbit plane normal and the Sun direction) especially in the case of ODY with larger excursions around the nominal value 1. This could not be attributed to, e.g. the self-shadowing effect which has been especially introduced for this spacecraft (proven by processing the data with and without this effect). The drag coefficients (same figure) stay rather below their nominal value for both spacecraft up to the beginning of 2004, and then exhibit large variations (even negative values) which have been unexplained; this may be a sign of lack of decorrelation with other parameters, enhanced over this time period by the weakness of the solar activity and an inadequate parameterization of the solar flux effect in the DTM-Mars model.

The quality of the orbit fits can also be judged from the differences in spacecraft positions between overlapping arcs, which we have investigated by reprocessing some of the data. The most interesting quantity is the radial component difference (e.g. in conjunction with the MOLA data — as used by the GSFC team); the smallest differences have been obtained for MGS during the GCO phase and have an RMS value of 6 cm, whereas values of one to five decimetres, depending on the time period, have been found with other data subsets (for MGS and ODY). Such figures can be compared with the quadratic mean of the radial orbit errors for MGS and ODY, computed from the full variance–covariance matrix of the MGGM08A solution (as in Balmino, 1992), and found to be ~1.3 cm (one sigma) for both spacecraft, a very small value indeed: a factor ~5 smaller than the best overlapping result during MGS-GCO. These findings are to be discussed later in assessing the realistic uncertainties of the recovered physical parameters.

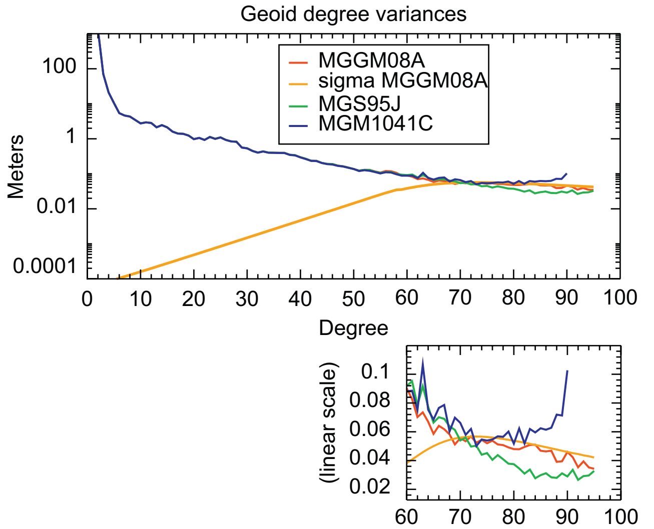

Fig. 4. RMS amplitudes of geoid heights (in m) per degree corresponding to MGGM08A and to the JPL and GSFC solutions. They are almost identical up to degree 60; then they slightly differ from each other (at centimetre level as shown in the 60–90 window with linear scale on the ordinate axis), which is probably due to different regularization power laws. Also represented are the geoid height RMS errors per degree, derived from the MGGM08A covariance matrix diagonal; they grow very regularly up to the degree where regularization starts, as expected.

4. The static gravity field of Mars

The sensitivity diagrams of Fig. 1 show that the analyzed orbits can together provide a full solution up to degree and order 50–60; higher degree-order terms induce significant perturbations though, thanks to resonance effects. The inversion up to $L = 95$ (which corresponds to the tiniest Doppler signals at the 50 μm/s level) needs being supplemented by a priori information. This comes from the Mars Kaula power rule, as used by all groups working in this domain; it provides a convenient regularization procedure by constraining the harmonics above a certain degree ($l = 58$ in our case) to zero with an uncertainty of $13 \times 10^{-5} l^{-2}$.

The model, named MGGM08A (for Mars Global Gravitational Model, year 2008, solution A) is a type 1 solution (static+10 days

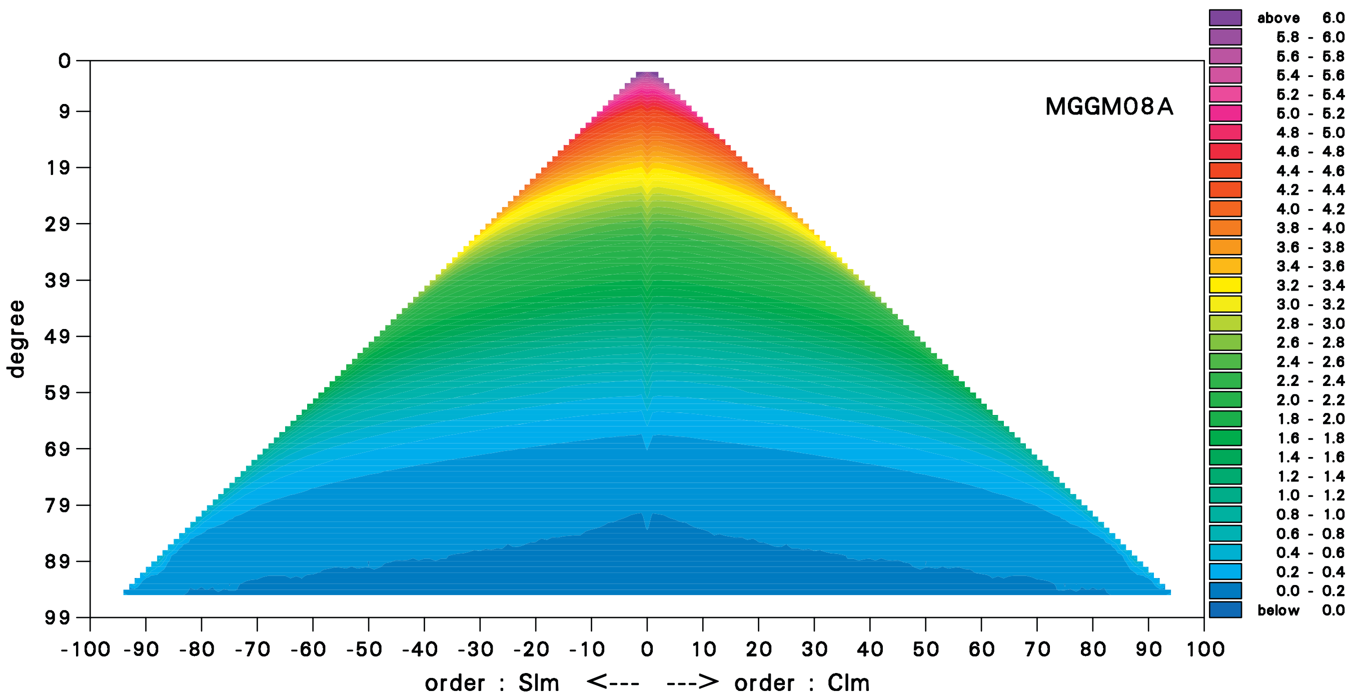

Fig. 5. Spherical harmonics formal errors relative to Kaula's rule for Mars. For each degree l and order m we map the function log10 $[(13.10{-}5/l^2)/\sigma_{lm}]$ where σ_{lm} is the formal error of C_{lm}, then S_{lm}. The color scale ranges from 0 (where the signal to noise ratio is *one*) to 6 (i.e. the error is *six* orders of magnitude below the signal).

time-varying J2 and J3). It can be compared to the modern NASA team solutions, MGS95J and GGM1041C, in different ways. Firstly, the recovered Mars GM value is $4.28283728 \times 10^{-13} \pm 0.000000034 \times 10^{-13}\,m^3\,s^{-2}$ for Mars GM, close to the value of 4.28283744 from Konopliv et al. (2006).

The next comparison may be based on the used data themselves and assessed in terms of orbit overlaps. This study was done for MGS for the whole year 2003 (with 4 days arcs overlapping by 2 h): The average of the total position differences decreases from 2.12 m with MGS95J to 1.96 m with MGGM08A.

Then, the harmonic coefficients themselves can be compared for instance in terms of geodetic quantities: as shown in Fig. 4 the RMS amplitudes of the geoid heights computed from the spherical harmonics degree variances appear to be very close between the three solutions (see Fig. 4); also the formal errors (one sigma) seem to be unrealistically small — to be discussed down below.

The error pattern of the coefficients themselves can be compared, as in Fig. 5 where the formal errors relative to Kaula's rule for Mars are displayed. The pattern is indeed undistinguishable from the one obtained from the errors provided with the MGS95J model (thus not shown). The errors increase regularly with the harmonic degree up to ~50–60 (as seen in Fig. 4 in a global way) and, generally, those of the coefficients close to the sectorials appear to be smaller than the others (of the same degree).

The map of the Martian geoid heights is shown in Fig. 6, and is extremely similar to maps of the MGM1041C and MGS95J geoids. Table 2 gives some insight on the differences, also for gravity anomalies, for the whole Mars and especially over the Tharsis-Valles Marineris area where the extreme values are encountered. The MGGM08A and MGS95J geoids are closer to each other (in terms of RMS differences) which may be explained by the truncation of MGM1041C at degree 90 (instead of 95 for the other models).

The interesting fact is that the RMS differences are significantly higher than, for instance, the formal geoid errors derived from the variance–covariance matrix and shown in Fig. 7. If we stick to the comparison between MGGM08A and MGS95J, we find an amplification of the formal errors by a factor ~9 for the whole Mars, and by a factor ~5 for the Tharsis-Valles Marineris area. In a somewhat optimistic approach, we also found a factor 5 in the best case when comparing the radial orbit errors derived in two different ways; we therefore recommend to adopt this factor *five* for scaling all formal errors obtained from our variance–covariance matrix.

It is of additional interest to study the correlations between the geoid heights and the Martian topography and, with a minimum of hypothesis, to show the remaining gravitational signal after removing the terrain effect. To do so we used the topography gridded values from Smith et al. (2001b) and performed a spherical harmonic analysis of these, thus obtaining a series of (dimensionless) coefficients (A_{lm}, B_{lm}) — after properly correcting for the elevation reference system. The correlation coefficients between these harmonics and the MGGM08A gravitational ones were found to be very close (above degree 40) to those computed by Konopliv et al. (2006)–who used the same topography source,

Table 2
Statistics of comparisons between the MGGM08A, MGM1041C and MGS95J geoids and gravity anomalies (after correcting for differences in the reference ellipsoid constants), for the whole Mars and for the Tharsis-Valles Marineris area.

Differences	Global			Tharsis-Valles Marineris*		
	Min	Max	RMS	Min	Max	RMS
Geoid						
MGGM08A–MGM1041C	−83	+94	14	−36	+54	8
MGGM08A–MGS95J	−73	+74	10	−46	+43	6
MGS95J–MGM1041C	−81	+97	13	−45	+48	8
Gravity anomalies						
MGGM08A–MGM1041C	−779	+792	128	−143	+219	42
MGGM08A–MGS95J	−648	+635	81	−233	+208	41
MGS95J–MGM1041C	−463	+691	90	−162	+170	42

Values are in meter for the geoid and in mgal for gravity anomalies (rounded). MGM1041C includes MGS data only, the two other models include MGS and ODY (and transition).

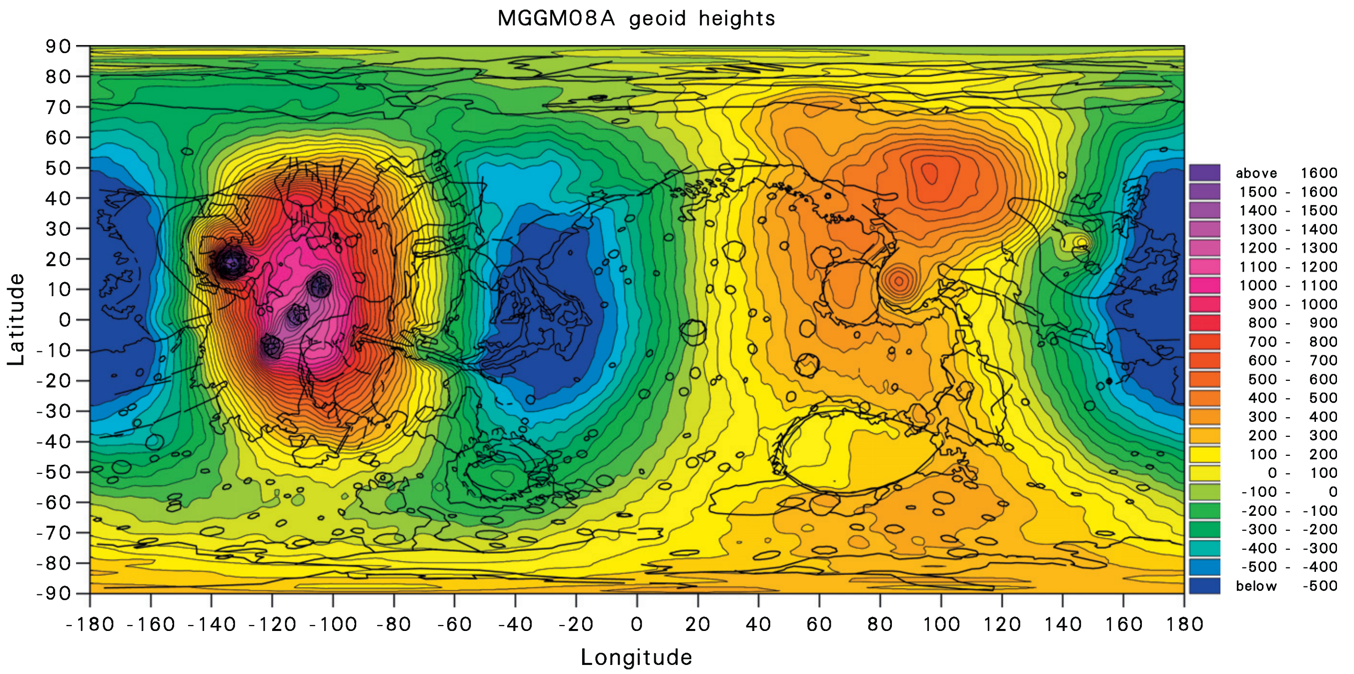

Fig. 6. Map of MGGM08A geoid heights, with respect to a reference ellipsoid with the following constants: equatorial radius = R, gravitational constant = GM as in the text; flattening = 1./191.1372, rotational rate = 7.0882181×10^{-5} rad/s. Max, min and RMS values are 1803, −756 and 340 m, respectively.

which is no surprise due to the similarity of the two gravity models. Then we derived the generalized isostatic gravitational field, of coefficients:

$$I_{lm} = G_{lm} - \Phi_l T_{lm} \quad (2)$$

with G_{lm} being the MGGM08A gravity harmonics (C_{lm}, S_{lm}), T_{lm} the topography harmonics (A_{lm}, B_{lm}), and Φ_l the transfer function coefficients defined by:

$$\Phi_l = \frac{\sum_m T_{lm} G_{lm}}{\sum_m T_{lm}^2} \quad (3)$$

where a general linear relationship is assumed in the spectral domain between gravity and topography (out from any physical hypothesis).

From the residual coefficients $I_{lm} = (\Delta C_{lm}, \Delta S_{lm})$, we derive the so-called generalized isostatic geoid shown in Fig. 8.

This approach leaves a much smoother residual geoid, also amplified over the Tharsis-Vales Marineris area (Fig. 9). It is worth noting that these isostatic geoid heights change by less than 10% (RMS) if one subtracts (in the spectral domain) the gravitational and topographic signatures of the large Tharsis volcanoes.

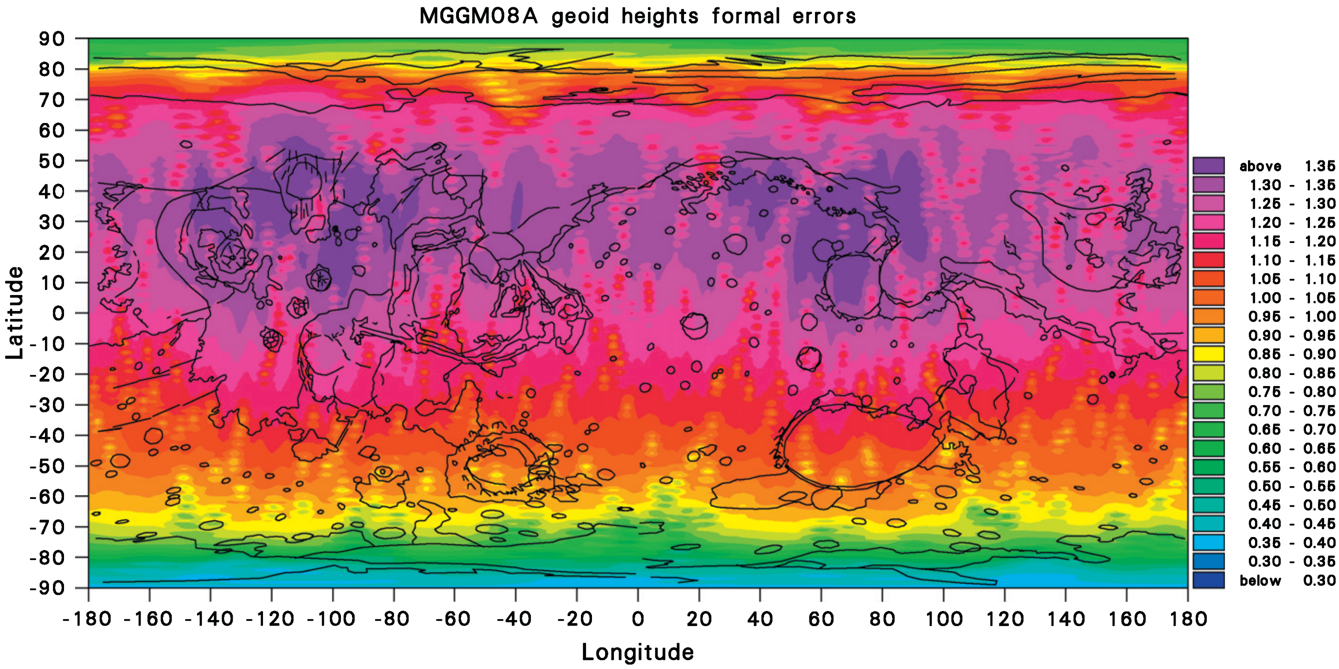

Fig. 7. Formal errors (in m, one *sigma*) mapped from the full variance-covariance matrix of the solution up to (95,95). Min, max and RMS values are 0.35, 1.42 and 1.15 m, respectively. A long wavelength zonal pattern is clearly seen (with smallest errors being at the poles), as well as shorter wavelength longitude dependant errors at the 1 m level (and slightly larger in the northern hemisphere).

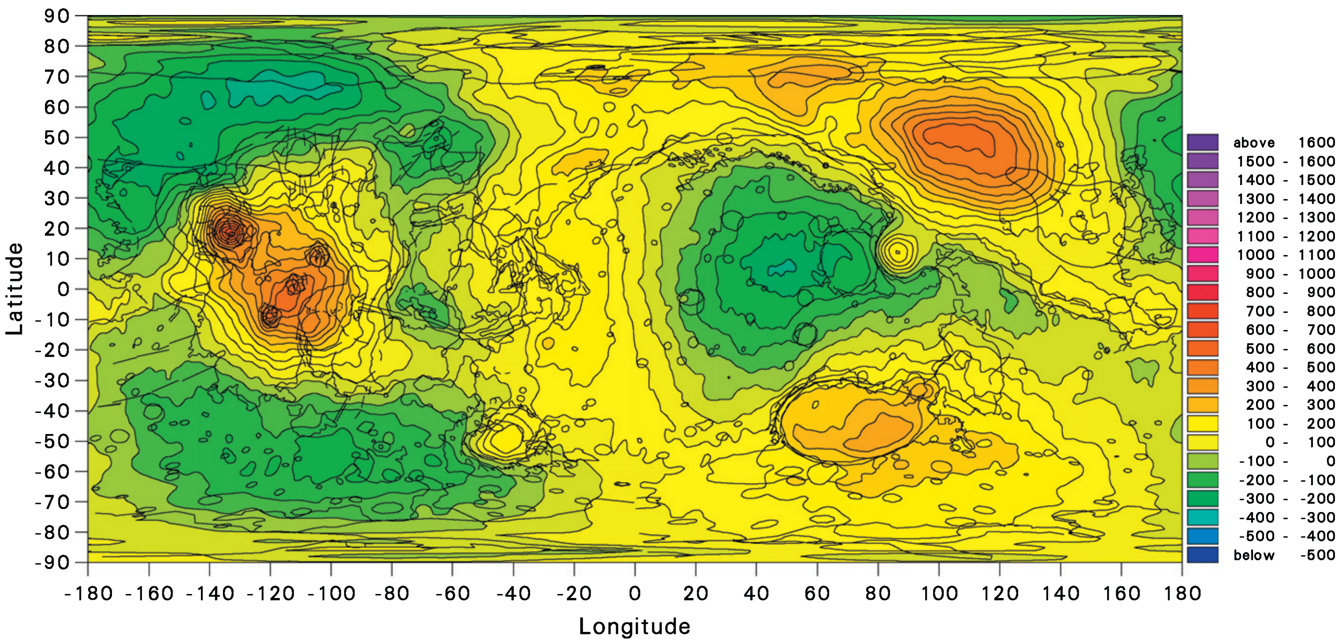

Fig. 8. Isostatic geoid derived by assuming a linear isotropic relationship between the gravitational potential and the topography. All harmonics are taken into account except the residual zonal coefficients up to degree *six*. Max, min and RMS values are 639, −332 and 141 m, respectively. The color scale is the same as in Fig. 6. A significant reduction (~60%) of the geoid variations is observed; the largest residual values are over Tharsis and Utopia Planitia.

The residual gravity field can be interpreted in terms of the apparent depth of compensation by degree, D_l, which is given by

$$D_l = \Phi_l \frac{2l+1}{l} \frac{g}{4\pi G \rho_0} \tag{4}$$

where g is the mean Martian surface gravity, ρ_0 the mean crust density (taken equal to 2800 kg/m^3) and G is as in (1); the factor $(2l+1)/l$ is sometimes replaced by $(2l+1)/(l+2)$ in some publications, which is the case when one does not take properly into account the spherical geometry (but this does not change much D_l as l increases). As seen in Fig. 10, between degrees 10 and ~75 the D_l's follow a simple linear law (which may not be used beyond degree ~60 due to the empirical regularization which was applied to the gravity solution); this tells us that some wavelength dependant isostatic compensation is taking place which may yield crustal thickness values if a proper isostatic model is introduced (see Neumann et al., 2004). For the longest wavelengths ($l<10$), the behaviour of these coefficients is very different, a sign that other mechanisms are (have been) at stake.

5. The variability of the zonal potential and the k_2 Love number

The determination of gravity harmonics from observations of a single type of orbits (the case of MGS and ODY which have very

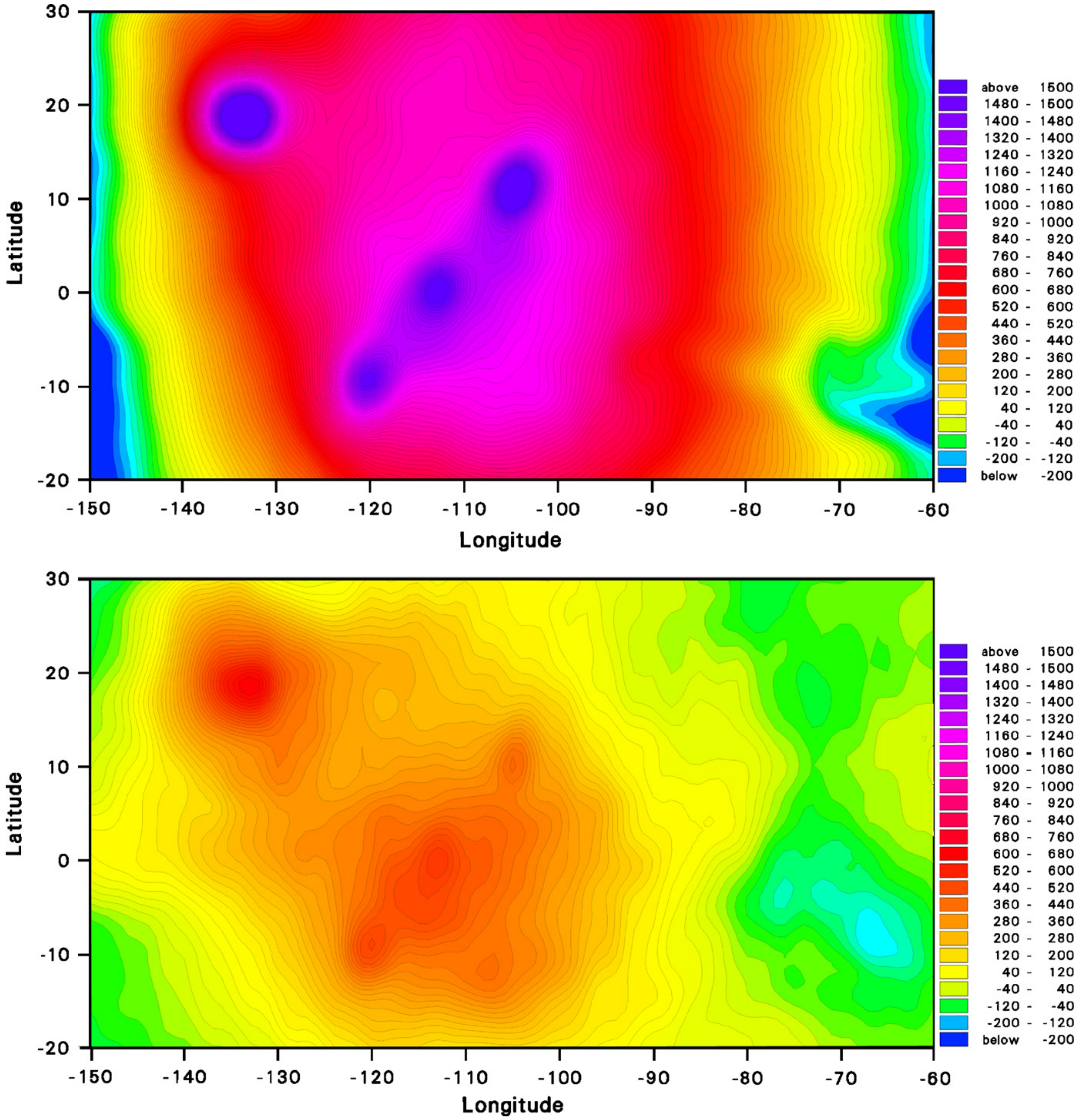

Fig. 9. MGGM08A geoid and isostatic geoid over the Tharsis-Valles Marineris area. Max, min and RMS values are: 1803, −293 and 742 m for the full geoid, and 639, −156 and 205 m, respectively.

similar elements) is hampered by the high correlations between coefficients of the same order m and different degrees l, which weaken the solution of the inverse problem. The rather dense coverage of the observations — and their quality, enable, though, the retrieval of a mean model at the 2–3% level of global relative precision (from Fig. 6 and Table 2). However, when it comes to the individual determination of some of the model coefficients — those being most impacted by time variations, the level of

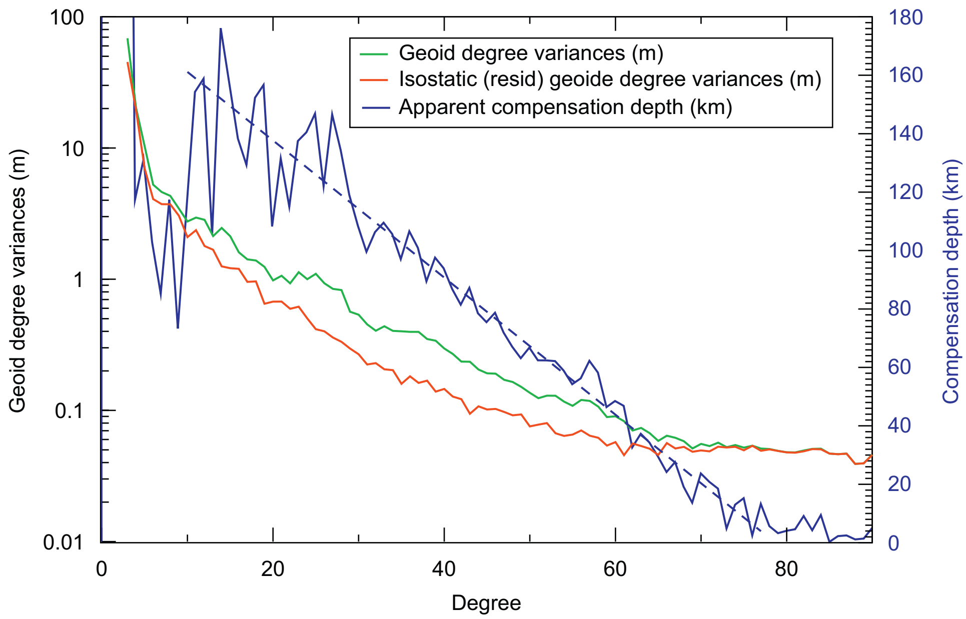

Fig. 10. Apparent depths of compensation D_l (between degrees 3 and 90) and degree variances of the isostatic geoid, showing the reduction from the original variances. The straight dotted line approximates the depths as $D_l = 185 - 2.35\,l$ (in km).

Table 3
Annual (A) and semi-annual (SA) amplitudes (in units of 10^{-9}) and phases (in degrees) of δC_{20} and δC_{30}, and comparisons with one solution of Balmino et al. (2005).

Solution	Lumped coeff.	A amplitude	A phase	SA amplitude	SA phase
MGGM08A (type 1 solution)	δC_{20}	3.51 ± 3.80	102 ± 12	2.78 ± 3.70	13 ± 15
	δC_{30}	1.83 ± 0.91	2 ± 6	0.57 ± 0.90	60 ± 19
Balmino et al. (2005)—MGS only (type 3 solution and forced periodic)	δC_{20}	0.60 ± 2.50	40 ± 57	0.10 ± 1.50	-9 ± 88
	δC_{30}	1.80 ± 2.00	4 ± 90	0.70 ± 1.50	63 ± 61

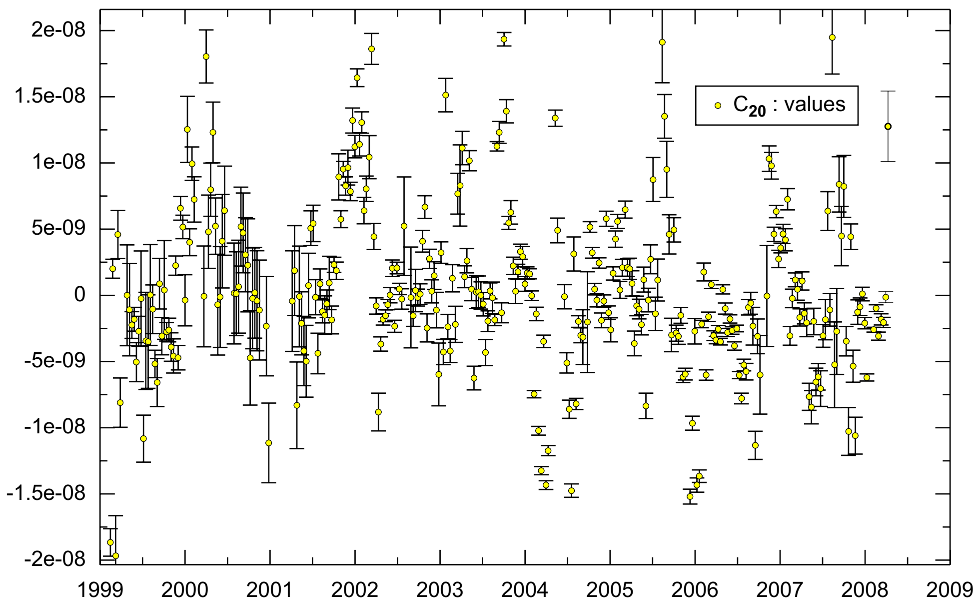

Fig. 11. Time variability of C_{20} with respect to the MGGM08A value, determined from the whole MGS and ODY data sets and together with the mean field (type 1 solution). Formal error bars (one *sigma*) show that the errors are in general much larger before ~2002–2003; they have been accounted for in the adjustment of periodic terms.

required precision increases dramatically. From predictions made from General Circulation Models, GCMs (Smith et al., 1999a, b; Karatekin et al., 2005; Sanchez et al., 2006), we know that a 10^{-5} or even 10^{-6} relative precision is already needed on the lowest degree zonal harmonics. From linear perturbation theory considerations (see for instance Balmino et al., 2005 or Karatekin et al., 2005) we know that it is not possible at such level and with the actual orbits to decorrelate the zonal coefficients of even degrees on the one hand, and those of odd degrees on the other hand; only the variations of the so-called lumped coefficients of degrees 2 and 3 may be retrieved with sufficient precision; these variations, which should have mainly annual and semi-annual signatures (from GCMs) will be denoted δC_{20} and δC_{30} in the following.

The second degree Love number, k_2, also produces annual and semi-annual perturbations (principally on the orbital plane), which may be in phase with those originating from δC_{20}. It is therefore necessary to estimate k_2 simultaneously, although correlations will decrease the accuracy with which both parameters are obtained.

Another concern, which comes from the perturbation theory, is the sensitivity of the observations to the perturbations on e, Ω and ω (orbital eccentricity, longitude of node, argument of periapsis, respectively), depending on the observer-orbit geometry. The orbital plane perturbations are much better seen (in the Doppler and range measurements) when the orbit is seen face-on, which favours the determination of δC_{20}. However, it reduces the ability to directly sense the in track non-conservative forces and it weakens the estimate of the variations in the orbit eccentricity and argument of periapsis. On the opposite, perturbations on (e, ω) are better mapped onto the observations when the orbit is seen edge-on, thus improving the determination of δC_{30}. In a pure

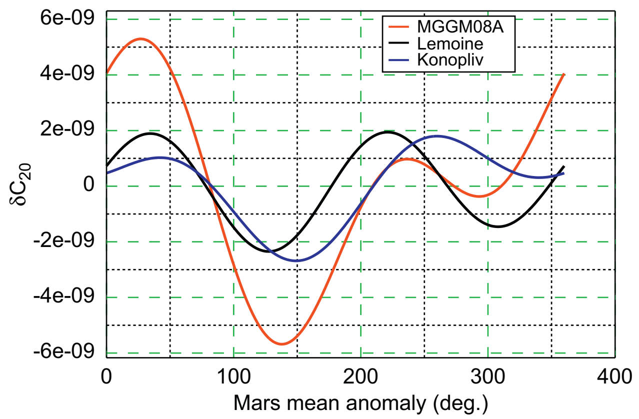

Fig. 12. Comparison of annual and semi-annual δC_{20} variations, in terms of Mars mean anomaly, obtained in three solutions: MGGM08A, Lemoine et al. (2006) and Konopliv et al. (2006). Our amplitudes are about twice higher than in the other two solutions but the phases are in reasonable agreement considering the uncertainties (see Table 3).

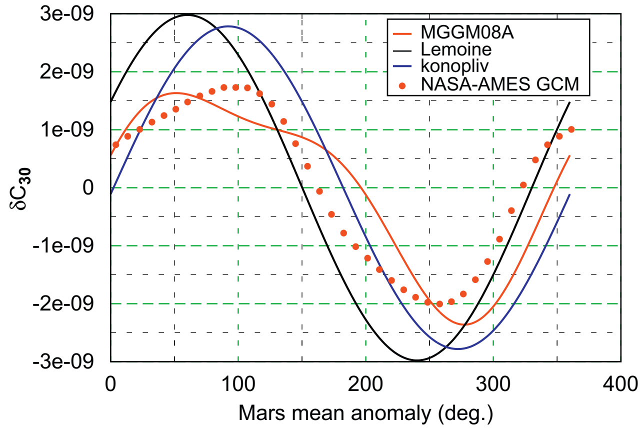

Fig. 14. Comparison of annual and semi-annual δC_{30} variations for three solutions (as in Fig. 13), with the series associated to the NASA-AMES GCM. The agreement is fairly good considering the (scaled) error of $\sim 0.9 \times 10^{-9}$ on each component (see Table 3).

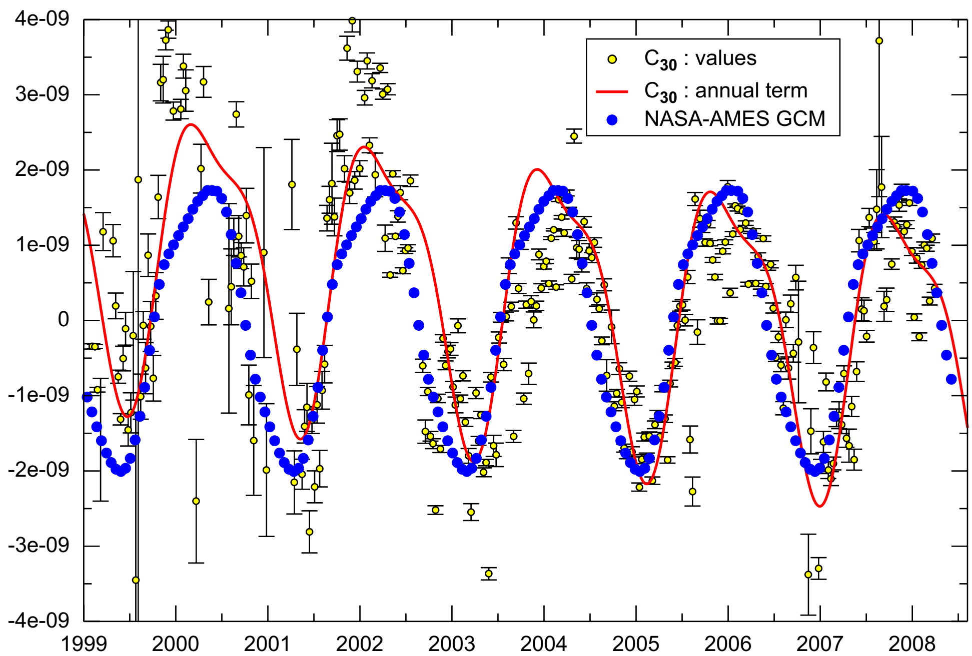

Fig. 13. Time series of δC_{30} with respect to the MGGM08A value, determined from the whole MGS and ODY data sets and together with the mean field. Formal error bars (one *sigma*) show, like for δC_{20}, that the errors are in general much larger before ~2002. Also shown are: the sum of the annual and semi-annual terms which have been a posteriori fitted, and the series derived from the NASA-AMES Global Circulation Model (Haberle et al., 1999).

numerical approach, as used in the present work, all variations in the orbital elements are analyzed, however, it is implicitly those on e, Ω and ω which bear more signal. Thanks to the two different orbital planes the geometry would be almost always favourable.

Finally by experimenting with variants of the AMD thrusts models and a priori variances, we realized, as pointed out earlier (e.g. Konopliv et al., 2006) that the precision in the recovery of k_2 and of the variability of C_{20} is limited by our ability at modelling the non-gravitational forces with sufficient accuracy and especially the AMD thrusts, the amount of degradation depending on the mission phases. The number of AMD per day is 4 or 5 for MGS before September 2001 and decreases to 1 or 2 after; for ODY there was one AMD per day only.

Several solutions for δC_{20} and δC_{30} were derived in different ways, all with an a priori uncertainty of 10^{-8} on each harmonic variation. Solution types 1 (static+time varying) and 3 (static only) gave similar results — though differing more from one another for δC_{20}. The errors to be associated to the results should correspond to the uncertainty in the whole model (type 1 solution); from our discussion in the previous section, the errors are multiplied by a factor 5.

For all non-forced periodic solutions annual and semi-annual terms are fitted a posteriori to the series of values (Table 3). We write those as: $\alpha_n \sin(nM_{Mars}+\varphi_n)$ with M_{Mars} being the mean anomaly of Mars and with $n=1$ and 2 for the annual and semi-annual variations respectively. We do not solve for ter-annual or higher order terms because we consider (from the graphs of the variations and from the realistic errors) that they cannot be reliably estimated.

The errors on the sine and cosine terms have been scaled up by a factor of 5 for MGGM08A as explained in the text, and those for the 2005 solution (one sigma) by a factor 5 too — somewhat arbitrary since the data set was different (MGS only) and shorter (5 years vs. 9.2 years in the present case). This shows the consistency of the δC_{30} series through the processing history of the MGS and Odyssey missions.

Fig. 11 shows the series of the δC_{20} recovered values for a type 1 solution (all parameters solved at the same time). As found before, e.g. by Konopliv et al. (2006) and ourselves (Balmino et al., 2005), the expected periodic signature is difficult to see. Forced periodic solutions do not look so much better unless being strongly constrained (at the 3×10^{-9} level) to a priori amplitudes (e.g. from a GCM) — which we do not advise to retain. The errors on the δC_{20} series are larger before 2002 (MGS only) thus we also derived a solution from the MGS and ODY data after March 2002, but this did not significantly modify the behaviour of the series over this reduced time span. We then compare the annual and semi-annual terms in three solutions over consecutive Martian years: we see in Fig. 12 that our amplitudes are larger than those in Konopliv et al. (2006) — where these amplitudes are directly

Table 4
Summary of k_2 Love number values obtained with different data subsets and/or in varying the strategy. MGS "part" stands for the data after April 2002.

Solution	Data set	k_2	Notes
Type 1	MGS (all)+ODY	0.116 ± 0.003	
Type 2	MGS (all)+ODY	0.107 ± 0.003	
Type 3	MGS (part)+ODY	0.120 ± 0.003	MGS: 2002–2006
Type 3	MGS (part)	0.050 ± 0.015	MGS: 2002–2006
Type 3	ODY	0.117 ± 0.004	
Yoder et al. (2003)	MGS	0.153 ± 0.017	MGS: 1999–April 2002
Balmino et al. (2005) type 3	MGS	0.130 ± 0.030	MGS: 1999–March 2005
Konopliv et al. (2006)	MGS+ODY	0.140 ± 0.009	Official MGS95J value
Duron et al. (2007)	MGS+ODY	0.120 ± 0.004	ODY until October 2007

Comparison with some independent results. The uncertainties have been scaled up by a factor of 5 for our solutions (this paper and the 2005 and 2007 solutions) as it was done in Yoder et al. (2003) and Konopliv et al. (2006). See Fig. 15 for a more complete history of the k_2 determination.

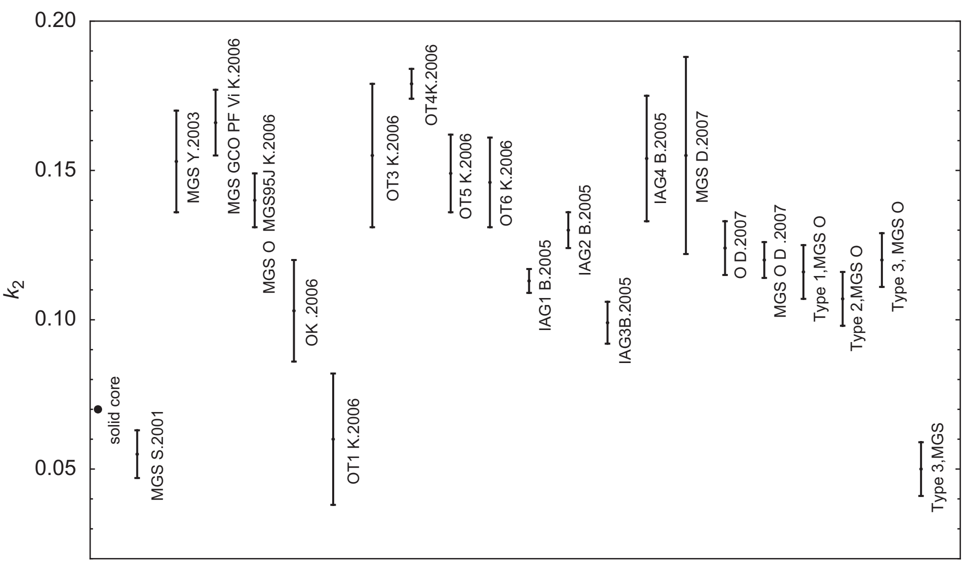

Fig. 15. History of the different values of k_2 obtained from MGS and Odyssey data analysis. The acronyms correspond to references. The error bars are those provided by their authors. The most recent ones (this paper, and Konopliv et al., 2006) correspond to formal uncertainties scaled up by a factor of 5.

the unknowns in the adjustment procedure, and are also larger than those obtained by Lemoine et al. (2006), by about a factor two; however, this is not incompatible with the errors in Table 3.

The results are indeed much more stable for δC_{30} which exhibits a definite periodic pattern (Fig. 13). Results of the periodic terms adjustment are given in Table 3, and the series of their sum is also shown in Fig. 13, together with the δC_{30} series provided by Haberle et al. (1999) with the NASA-AMES GCM. As above we finally compare the annual and semi-annual terms behaviour (function of Mars mean anomaly) for three solutions and with the GCM's δC_{30} (Fig. 14); we find a closer agreement between the latter and our solution.

The values of k_2 obtained in different configurations and according to the parameterization and initial models described in Section 2, are summarized in Table 4. Apart from a small value obtained in a type 3 solution with MGS data only (and which could not be explained), all other values are quite consistent. The earlier determinations, based on shorter data spans, and suffering from a large number of AMD events (for MGS) may be considered less reliable. Among our solutions we favour the one derived from the ODY and the MGS data since 2002 (it is a type 3 solution) because of the correlation between k_2 and δC_{20} and, as noted above, due to the largest error bars on the δC_{20} series before 2002; this value is 0.120 ± 0.003.

In Fig. 15, we compare the most recent values of k_2 with all those previously obtained, with different approaches and data sets (shorter, or much shorter than the present one). We see a clear accumulation of values between 0.11 and 0.17, suggesting that Mars has a fluid core (a solid core is associated with a value of ~0.07).

In Fig. 16, the k_2 Love number is shown as a function of core radius for theoretical models of the Martian interior with different crust densities (2700–3200 kg/m^3) and thicknesses (20–100 km), the DW mantle mineralogy (Dreibus and Wänke, 1985) and two mantle temperature end-members. For the range of the k_2 estimates between 0.120 and 0.140 (from our results and those from Konopliv et al. 2006), the size of the core ranges between about 1500 and 1800 km. The broadness of the curves in Fig. 16 results from the chosen range of crust thickness and density, which reflects the uncertainty on these two parameters. This uncertainty has only a minor effect on the k_2 value, and in turn the crust cannot be constrained given the level of precision on the k_2 estimates. Both the preferred k_2 solutions, ours and Konopliv et al.'s (2006) ones, are in favour of a fully molten core for both mantle temperature end-members and the DW mantle mineralogy. Our k_2 value, results in somewhat smaller core sizes than those derived from the k_2 values of Konopliv et al. (2006) and Yoder et al. (2003). As a consequence, with our k_2 value, it is more likely that the pressure in the deep mantle is high enough for the phase transition to perovskite to occur, which is one of the possible conditions for the formation of plume-like features explaining the presence of long standing volcanoes at the planetary surface, such as those in the Tharsis region (van Thienen et al., 2006).

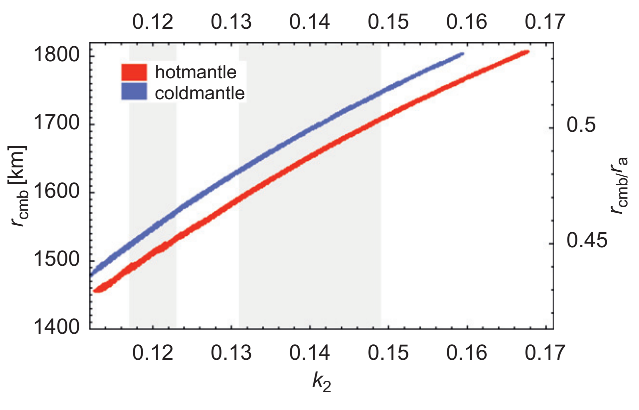

Fig. 16. Core radius r_{CMB} of Mars as a function of tidal Love number k_2, for the DW mantle mineralogy and two temperature end-members (red for hot and blue for cold). The crust density and thickness are in the range [20,100] km to [2700,3200] kg/m^3, and result in the broadening of the curves. Both gray shaded areas correspond to the uncertainty domains of our preferred k_2 solutions and Konopliv et al.'s (2006) one.

6. Conclusions

We have derived a new global mean gravity field model of Mars and large-scale time variations from the analysis of 9.2 years of data from the MGS and Odyssey missions, which is the longest data set ever analyzed for this purpose. The static field is very close to other modern solutions and within the errors estimated in the inverse problem. It can be used for further geophysical interpretation, for instance starting from the generalized isostatic field which has also been derived (using an up to date Martian topographic model). Seasonal variations of the gravity field in the (lumped) zonal harmonics of degrees 2 and 3 have been confirmed; the degree 2 coefficient variations which we have derived are still quite noisy, whereas the degree 3 variability comes out very clean and we are confident that our determination has strengthened its knowledge thanks to the observation time span (almost 5 Martian years). The degree 2 Love number value is in the range 0.110–0.130 depending on the solutions. Considering the uncertainties derived from formal statistics and external considerations, taking also into account solutions obtained by other authors, we state that k_2 lies between 0.110 and 0.160; this supports the hypothesis of a fluid core of Mars and favour the presence of a perovskite layer at the bottom of the mantle.

New sets of data from Mars Reconnaissance Orbiter (MRO) are now available. They could provide us new constraints on k_2 and seasonal variations of the gravity field of Mars.

Acknowledgments

This study used the GINS software and DYNAMO libraries developed by the Satellite Geodesy team at CNES. We acknowledge F.G. Lemoine and D.D. Rowlands (GSFC) for providing assistance and software for handling the MGS spacecraft attitude. MGS and Odyssey Radio Science team members and especially Dick Simpson (Stanford University) are thanked for their help in providing data and advises. We are grateful to Nicole Vales who was very helpful in producing many of the graphics. This research was supported by the CNES Programme Directorate and the Toulouse Space Center on one hand, and by the Royal Observatory of Belgium (ROB) on the other hand. The work at ROB was financially supported by the Belgian PRODEX program managed by the European Space Agency in collaboration with the Belgian Federal Science Policy Office. ROB benefited also from Action-2 grants of the Belgian Science Federal Policy and from the support of the European's Community Improving Human Potential Programme, under Contract RTN-2001-00414, MAGE.

References

Balmino, G., Moynot, B., Vales, N., 1982. Gravity field model of mars in spherical harmonics up to degree and order eighteen. J. Geophys. Res. 87 (B12), 9735–9746.

Balmino, G., 1992. Orbit choice and the theory of radial orbit error for altimetry. In: Rummel, R., Sanso, F. (Eds.), Satellite Altimetry in Geodesy and Oceanography. Springer, Berlin, New York, pp. 243–315.

Balmino, G., Duron, J., Marty, J.C., Karatekin, Ö., 2005. Mars long wavelength gravity field time variations; a new solution from MGS tracking data. In: Proceedings of the IAG-IAPSO-IABO General Assembly on 'Dynamic Planet' 2005, Cairns, Australia, Proceedings Series. Springer, Berlin, New York, pp. 895–902 (Chapter 125).

Bruinsma, S., Lemoine, F.G., 2002. A preliminary semiempirical thermosphere model of Mars: DTM-Mars. J. Geophys. Res. 107 (E10).

Dreibus, G., Wänke, H., 1985. Mars: a volatile-rich planet. Meteoritics 20, 367–382.

Duron J., Marty, J.C., Balmino, G., Rosenblatt, P., Le Maistre, S., Dehant, V., 2006. Time variations of Mars gravity field from Mars Global Surveyor and Odyssey data. A.G.U. Fall meeting, Planetary Geodesy, P31C-0157.

Duron, J., Marty, J.C., Balmino, G., Rosenblatt, P., Le Maistre, S., Dehant, V., 2007. Martian gravity field mean model and its time variations from Mars Global Surveyor and Odyssey data. A.G.U. Fall meeting, Planetary Sciences, P41A-0186.

Folkner, W.M., Kahn, R.D., Preston, R.A., Yoder, C.F., Standish, E.M., Williams, J.G., Edwards, C.D., Hellings, R.W., Eubanks, T.M., Bills, B.G., 1997. Mars dynamics from Earth-based tracking of the Mars pathfinder lander. J. Geophys. Res. 102, 4057–4064.

Haberle, R.M., Joshi, M.M., Murphy, J.R., Barnes, J.R., Schofield, J.T., Wilson, G., Lopez-Valverde, M., Hollingsworth, J.L., Bridger, A.F.C., Schaeffer, J., 1999. General circulation model simulations of the Mars pathfinder atmospheric structure investigation/meteorology data. J. Geophys. Res. 104 (E4), 8957–8974.

Karatekin, Ö., Duron, J., Rosenblatt, P., Van Hoolst, T., Dehant, V., Barriot, J.P., 2005. Mars' time-variable gravity and its determination: simulated geodesy experiments. J. Geophys. Res. (Planets) 110 (E6), E06001.

Kaula, W.M., 1966. Theory of Satellite Geodesy. Blaisdell, Waltham, MA.

Konopliv, A.S., Sjogren, W.L., 1995. The JPL Mars gravity field, Mars50c, based upon Viking and Mariner 9 Doppler tracking data, JPL Publ. 95–5, Jet Propul. Lab., Pasadena, California.

Konopliv, A.S., Yoder, C.F., Standish, E.M., Yuan, D.-N., Sjogren, W.L., 2006. A global solution for the Mars static and seasonal gravity, Mars orientation, phobos and deimos masses, and Mars ephemeris. Icarus 182, 23–50.

Lainey, V., Dehant, V., Pätzold, M., 2007. First numerical ephemerides of the two martian moons. Astronom. Astrophys. 465 (3), 1075–1084.

Lemoine, F.G., 1992, Mars: The dynamics of orbiting satellites and gravity model development. Ph.D. Thesis, University of Colorado, Boulder, CO.

Lemoine, F.G., Smith, D.E., Rowlands, D.D., Zuber, M.T., Neumann, G.A., Chinn, D.S., Pavlis, D.E., 2001. An improved solution of the gravity field of Mars (GMM-2B) from Mars Global Surveyor. J. Geophys. Res. 106 (E10), 23359–23376.

Lemoine, F.G., Bruinsma, S., Chinn, D.S., Forbes, J.M., 2006. Thermospheric studies with Mars Global Surveyor. Paper Presented at AIAA/AAS Astrodynamics Specialist Conference. American Institute of Aeronautics and Astronautics, Keystone, Colorado.

Mazarico, E., Zuber, M., Lemoine, F., Smith, D., Improved force modeling on Mars-Orbiting spacecraft. In: Proceedings of the AIAA/AAS Astrodynamics Specialist Conference, paper AIAA-2008-7201, Honolulu, Hawaii, August 18–21, 2008.

McCarthy, D.D. (Ed.), 1996. IERS Technical Note 21, US Naval Obs., Washington, DC.

Moyer, T.D., 2000. Formulation for observed and computed values of Deep Space Network data types for navigation, Monograph 2, Deep Space Communications and Navigation Series.

Neumann, G.A., Zuber, M., Wieczorek, M.A., McGovern, P.J., Lemoine, F.G., Smith, D.E., 2004. Crustal structure of Mars from gravity and topography. J. Geophys. Res. 109, E08002.

Neumann, G.A., Rowlands, D.D., Lemoine, F.G., Smith, D.E., Zuber, M.T., 2001. Crossover analysis of Mars Orbiter laser altimeter data. J. Geophys. Res. 106, 23753–23768.

Rosenblatt, P., Lainey, V., Le Maistre, S., Marty, J.C., Dehant, V., Pätzold, M., Van Hoolst, T., Häusler, B., 2008. Accurate Mars express orbits to improve the determination of the mass and ephemeris of the martian moons. Planet. Space Sci. 56, 9.

Sanchez, B.V., Rowlands, D.D., Haberle, R.M., 2006. Variations of Mars gravitational field based on the NASA/Ames general circulation model. J. Geophys. Res. (Planets), 111, E06010, doi:10.1029/2005JE002442.

Seidelmann, P.K., Abalakin, V.K., Bursa, M., Davies, M.E., De Bergh, C., Lieske, J.H., Oberst, J., Simon, J.L., Standish, E.M., Stooke, P., Thomas, P.C., 2002. Report of the IAU/IAG working group on cartographic coordinates and rotational elements of the planets and satellites: 2000. Celest. Mech. Dynam. Astron. 82, 83–111.

Sjogren, W.L., Yuan, D.-N., Konopliv, A.S., 1999. Mars gravity field modeling with MGS, Spring meeting. Eos Trans. AGU 80(17) (Suppl.) S204.

Smith, D.E., Lerch, F.J., Nerem, R.S., Zuber, M.T., Patel, G.B., Fricke, S.K., Lemoine, F.G., 1993. An improved gravity model for Mars: Goddard Mars model 1. J. Geophys. Res. 98 (E11), 20871–20889.

Smith, D.E., Sjogren, W.L., Tyler, G.L., Balmino, G., Lemoine, F.G., Konopliv, A.S., 1999a. The gravity field of Mars: results from Mars Global Surveyor. Science 286, 94–97.

Smith, D.E., Zuber, M.T., Haberle, R.M., Rowlands, D.D., Murphy, J.R., 1999b. The Mars seasonal CO_2 cycle and the time variation of the gravity field: a general circulation model simulation. J. Geophys. Res. 104 (E1).

Smith, D.E., Zuber, M.T., Neumann, G.A., 2001a. Seasonal variations of snow depth on Mars. Science 294, 2141–2146.

Smith, D.E., Zuber, M.T., Frey, M.T., Garvin, J.B., Head, J.W., Muhleman, D.O., Pettengill, G.H., Phillips, R.J., Solomon, S.C., Zwally, H.J., Banerdt, W.B., Duxbury, W.B., Golombek, M.P., Lemoine, F.G., Neumann, G.A., Rowlands, D.D., Aharonson, O., Ford, P.G., Ivanov, A.B., Johnson, C.L., McGovern, P.J., Abshire, J.B., Afzal, R.S., Sun, X., 2001b. Mars orbiter laser altimeter: experiment summary after the first year of global mapping of Mars. J. Geophys. Res. 106 (E10), 23689–23722.

Smith, D.E., Zuber, M.T., 2003. Seasonal changes in the masses of the polar ice caps of Mars as derived from Mars Global Surveyor gravity. Abstract of 'Mars Atmosphere Modelling and Observations' Workshop, Granada, Spain, 13–15 January.

Standish, E.M., 2006. JPL Planetary Ephemeris DE414. JPL Technical Report IOM 343R-06-002, April 21, 2006.

Tyler, G.L., Balmino, G., Hinson, D.P., Sjogren, W.L., Smith, D.E., Simpson, R.A., Asmar, S.W., Priest, P., Twicken, J.D., 2001. Radio science observations with Mars Global Surveyor: orbit insertion through one Mars year in mapping orbit. J. Geophys. Res. 106 (E10), 23327–23348.

Van Thienen, P., Rivoldini, A., Van Hoolst, T., Lognonné, P., 2006. A top-down origin for martian mantle plumes. Icarus 185 (1), 197–210.

Yoder, C.F., Konopliv, A.S., Yuan, D.N., Standish, E.M., Folkner, W.M., 2003. Fluid core size of Mars from detection of the solar tide. Science 300, 299–303.